ACS MATERIALS Au
AN OPEN ACCESS JOURNAL OF THE AMERICAN CHEMICAL SOCIETY

pubs.acs.org/materialsau

Article

$(NH_4)_2AgX_3$ (X = Br, I): 1D Silver Halides with Broadband White Light Emission and Improved Stability

Tielyr D. Creason,[§] Hadiah Fattal,[§] Isaiah W. Gilley, Timothy M. McWhorter, Mao-Hua Du, and Bayram Saparov*

Cite This: https://doi.org/10.1021/acsmaterialsau.1c00009

Read Online

ACCESS | Metrics & More | Article Recommendations | Supporting Information

ABSTRACT: Recently, ternary copper(I) halides have emerged as alternatives to lead halide perovskites for light emission applications. Despite their high-efficiency photoluminescence (PL) properties, most copper(I) halides are blue emitters with unusually poor tunability of their PL properties. Here, we report the impact of substitution of copper with silver in the high-efficiency blue-emitting Cu(I) halides through hydrothermal synthesis and characterization of $(NH_4)_2AgX_3$ (X = Br, I). $(NH_4)_2AgX_3$ are found to exhibit contrasting light emission properties compared to the blue-emitting Cu(I) analogues. Thus, $(NH_4)_2AgBr_3$ and $(NH_4)_2AgI_3$ exhibit broadband whitish light emission at room temperature with PL maxima at 394 and 534 nm and full width at half-maximum values of 142 and 114 nm, respectively. Based on our combined experimental and computational results, the broadband emission in $(NH_4)_2AgX_3$ is attributed to the presence of high-stability self-trapped excitons and defect-bound excitons. $(NH_4)_2AgBr_3$ and $(NH_4)_2AgI_3$ both have significantly improved air and moisture stability as compared to the related copper(I) halides, which are prone to degradation via oxidation. Our results suggest that silver halides should be considered alongside their copper analogues for high-efficiency light emission applications.

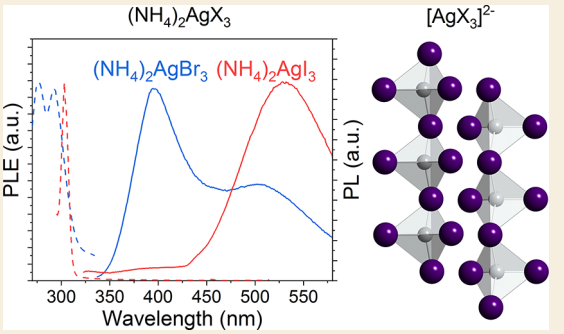

KEYWORDS: *Photoluminescence, lead−free halides, silver halides, light emission, STE*

INTRODUCTION

Novel ternary metal halides have garnered significant attention in the past decade for prospective light emission applications such as solid-state lighting and radiation detection.[1−5] Among the most prominent examples are cesium and methylammonium lead halide perovskites, particularly in their nanoparticle forms, demonstrating tunable and highly efficient light emission properties.[2,6−9] However, the toxic nature of lead poses a challenge from an environmental perspective, and lead halide perovskites are known to exhibit poor stability in ambient air conditions.[8,10,11] Furthermore, the preparation of high-quality nanoparticles of lead halide perovskites involves lengthy and complicated synthesis methods.[6−9,12] These challenges hinder the prospects of lead halide perovskites for commercialization and use in practical applications.

High-efficiency light emitters based on lead-free alternative metal halides have been developed in the past few years in the form of ternary copper(I) halides. Notable examples include compounds such as $Cs_3Cu_2X_5$ (X = Cl, Br, or I) and A_2CuX_3 (A = K or Rb, X = Cl or Br), which were found to have record-breaking blue light emission efficiencies with room temperature photoluminescence quantum yield (PLQY) values up to 100%.[4,13−18] Of these, A_2CuX_3 compounds have been attracting attention due to recent improvements in their stability and demonstration of their potential in radiation detection applications.[14,18] Light emission in these low-dimensional copper(I) halides, including the A_2CuX_3 family, has been attributed to self-trapped excitons (STEs), which are formed through structural reorganizations that occur in the excited state, leading to charge localization on distorted metal halide polyhedra.[19,20] These trapped excitons form midgap states that have significantly red-shifted the emission peaks relative to the absorption energies. Such exciton trapping is ubiquitously observed in lower-dimensional metal halides as the energy barrier is lower for structural distortion, emphasizing the roles of chemistry and structural dimensionality in the photoemission properties of metal halides. Despite their outstanding optical emission properties, the members of the A_2CuX_3 family are all blue emitters and substitutions on the A and X sites in A_2CuX_3 have shown only negligible impacts on the optical properties.[13,14,17,18,20] Such unusual lack of tunability of the photoluminescence (PL) properties in the A_2CuX_3 family is due to the fact that electronic transitions take

Received: April 7, 2021

place primarily between copper(I) orbitals.[13,14] To bring PL tunability to this family, a strategy based on the substitution of Cu(I) with alternative metals (e.g., with Ag) is proposed. The validity of this approach was recently demonstrated for the A_2AgX_3 (A = Rb, Cs; X = Cl, Br), which exhibit tunable broadband emission spectra attributed to STEs and defect-bound excitons (DBEs).[21,22] Independent from the A_2AgX_3 family, there has also been an increasing interest in hybrid variants of ternary silver halides, such as the white light emitting $(H_2DABCO)[Ag_2X_4(DABCO)]$ and $(HDABCO)_3Ag_5Cl_8$.[23] These all-inorganic and hybrid compounds have set the stage for ternary silver halides as potential white light emitters, with high PLQY values up to 27%.[21]

Here, we report the preparation and characterization of $(NH_4)_2AgX_3$ (X = Br and I). Although not isostructural, $(NH_4)_2AgX_3$ exhibit very similar structures to that of A_2CuX_3, based on 1D $[AgX_3]^{2-}$ chains made of tetrahedral AgX_4 units separated by NH_4^+ cations.[24] Substitution of alkali metal cations with NH_4^+ is both cost-effective and removes the issues associated with the intrinsic radioactivity of alkali metals such as Rb used in Rb_2CuX_3, expanding the potential of $(NH_4)_2AgX_3$ for radiation detection applications. Large centimeter-sized colorless needles were synthesized through a hydrothermal preparation method. Both single crystal and powder X-ray diffraction methods were used to characterize structure and bulk purity. In stark contrast to Cu(I) analogues, $(NH_4)_2AgX_3$ exhibit white light emission properties. Detailed investigations, including density functional theory (DFT) calculations and optical spectroscopy measurements, were performed to elucidate the white light emission mechanism. Based on our combined experimental and computational work, low dimensional silver halides constitute an exciting new family of nontoxic and rare-earth-free luminescent metal halides with tunable optical properties.

EXPERIMENTAL SECTION

Materials and Methods

The starting reactants: ammonium bromide (>99.99%, Aldrich), silver bromide (99.5%, Alfa Aesar), ammonium iodide (>99%, Sigma-Aldrich), and silver iodide (99.999%, Alfa Aesar) were used as received. All solvents were obtained via Sigma-Aldrich and used as received, including hypophosphorous acid (50%), hydrobromic acid (48%), and hydroiodic acid (47%). All manipulations of reactants and products were performed in a nitrogen-filled glovebox.

$(NH_4)_2AgX_3$ Single Crystals via Slow Cooling of a Saturated Solution

$(NH_4)_2AgX_3$ single crystals measuring up to 1.5 cm in length were prepared by mixing stoichiometric amounts of NH_4X (X = Br, I) and AgX in a 6 M HX solution. A combined 1.5 g of reagents was added to a 20 mL glass scintillation vial wrapped in an aluminum foil, then 10.0 mL of the corresponding acid was added. H_3PO_2 (~5% by volume) was added to the resultant solution. The vial was then capped, placed in the center of a box furnace, and heated at 130 °C until all reactants fully dissolved, producing a clear solution. The box furnace was held at 130 °C for 6 h, followed by slow cooling to 25 °C over 105 h. The obtained products are composed of long colorless needle crystals of $(NH_4)_2AgX_3$ with binary AgX impurity crystals on the surface as confirmed by the powder X-ray diffraction (PXRD) measurements. Therefore, for characterization of optical properties, larger needle crystals with minimal surface impurities were carefully collected and repeatedly washed in isopropyl alcohol (see Figure S1).

Powder X-ray Diffraction (PXRD) Measurements

To establish the samples' bulk purity, PXRD measurements were taken on a Rigaku Miniflex600 instrument equipped with a D/tex detector and a Ni-filtered Cu Kα radiation source. Data were collected at room temperature in the 3−90° (2θ) range, with a step size of 0.02°. The obtained PXRD patterns were refined using the decomposition method. To test the air stability of $(NH_4)_2AgX_3$, powdered samples were left on a laboratory bench under ambient conditions (thermostat set at 20 °C and relative humidity of 30%), and periodic PXRD experiments were performed to monitor the changes. The reference intensity ratio (RIR) quantitative analysis was performed using the PDXL2 program to quantify the sample composition changes.

Single Crystal X-ray Diffraction (SCXRD)

Single crystal X-ray diffraction (SXRD) data were collected on a Bruker D8 Quest system with a Kappa geometry goniometer, an Incoatec IμS X-ray source (graphite monochromated Mo Kα (λ = 0.71073 Å) radiation), and a Photon II detector. The data were corrected for absorption using the semiempirical method based on equivalent reflections, and the structures were solved by intrinsic phasing methods (SHELXT) as embedded in the APEX3 v2015.5-2 program. Site occupancy factors were checked by freeing occupancies of each unique crystallographic positions. Details of the data collection and crystallographic parameters are given in Table S1. Atomic coordinates, equivalent isotropic displacement parameters, and selected interatomic distances and bond angles are provided in Tables S2 and S3 in the Supporting Information (SI). Additional information on the crystals structures investigations can be obtained in the form of a Crystallographic Information File (CIF), which was deposited in the Cambridge Crystallographic Data Centre (CCDC) database (deposition numbers 2031391 and 2031392).

Microscopy

A Thermo Quattro S field-emission environmental scanning electron microscope (FE-ESEM) was utilized to obtain the SEM images. Optical images of crystals were captured on a Leica S6D microscope with a Leica EC4 digital camera attachment.

Thermogravimetry and Differential Scanning Calorimetry (TGA/DSC) Measurements

Simultaneous thermogravimetric analysis and differential scanning calorimetry (TGA/DSC) measurements were performed on a TA Instruments SDT 650 thermal analyzer system. Polycrystalline powder samples of $(NH_4)_2AgX_3$ (~15 mg) were placed in 90 μL alumina crucibles with the corresponding caps and heated from 25 to 450 °C with a heating rate of 5 °C/min under an inert flow of dry nitrogen gas at a rate of 100 mL/min.

Optical Measurements

Room temperature photoluminescence emission (PL) and photoluminescence excitation (PLE) measurements were performed on single crystals of $(NH_4)_2AgX_3$ on a Jobin Yvon Fluorolog-3 spectrofluorometer (HORIBA company) equipped with a xenon lamp with a range from 280 to 750 nm. Commission Internationale de l'Eclairage (CIE) color coordinates were generated from PL spectra in Origin 2019. For lifetime measurements, a time-correlated single photon counting (TCSPC) system including a DeltaHub DH-HT high throughput TCSPC controller and NanoLED NL-C2 pulsed diode controller was used. A 299 nm NanoLED diode was selected for the light source, which has a <1.2 ns pulse duration. In order to fit the data, the following equations were used:

$$I(t) = \sum_i^n \alpha_i \exp\left(\frac{-t}{\tau_i}\right)$$

$$\alpha_1 = \frac{B_1}{(B_1 + B_2)} \quad \alpha_2 = \frac{B_2}{(B_1 + B_2)}$$

The fitting parameters calculated in this study are available in Table S4.

Computational Methods

Our calculations were based on DFT as implemented in the VASP code.[25] The kinetic energy cutoff of the plane-wave basis is 400 eV.

https://doi.org/10.1021/acsmaterialsau.1c00009
ACS Mater. Au XXXX, XXX, XXX−XXX

The projector augmented wave method was used to describe the interaction between ions and electrons.[26] The lattice parameters were fixed at the experimentally measured values while the atomic positions were optimized until the force on each atom is less than 0.02 eV/Å. The electronic band structure and density of states (DOS) were calculated using Perdew−Burke−Ernzerhof (PBE) exchange-correlation functional[27] and the band gap was further corrected using the hybrid PBE0 functional.[28]

RESULTS AND DISCUSSION

$(NH_4)_2AgBr_3$ and $(NH_4)_2AgI_3$ are isostructural compounds crystallizing with the K_2AgI_3 type structure in the *Pnma* space group (Tables S1−S3).[24] Their structure consists of $1D^1_\infty[AgX_3]^{2-}$ tetrahedral chains extending along the *b*-axis, which are separated by $[NH_4]^+$ ions (Figure 1). $(NH_4)_2AgBr_3$ has Ag−Br bond lengths ranging from 2.6934(3) to 2.7139(6) Å and Br−Ag−Br angles ranging from 101.239(19) to 109.664(14)°. These are fairly similar to those for Rb_2AgBr_3, where Ag−Br bond lengths range from 2.6925 to 2.7224 Å and Br−Ag−Br angles range from 103.65 to 117.14°. Compared to $(NH_4)_2AgBr_3$, $(NH_4)_2AgI_3$ features slightly less distorted tetrahedra, with Ag−I bond lengths ranging from 2.8345(7) to 2.8647(4) Å and I−Ag−I angles from 104.982(19) to 109.505(12)°. These bond lengths are within the expected range and are consistent with that reported for K_2AgI_3, where Ag−I bond lengths range from 2.8093 to 2.8525 Å and I−Ag−I angles are from 103.90 to 113.83°.[29] Note that the K_2AgI_3 type structure is similar to the K_2CuCl_3 type structure adopted by the A_2CuX_3 family, which have recently been reported as ultrabright blue emitters with prospective applications in solid-state lighting and radiation detection applications.[4,13,14,17] The differences between the two structure types are in the packing of the chains relative to the A cationic site.[24]

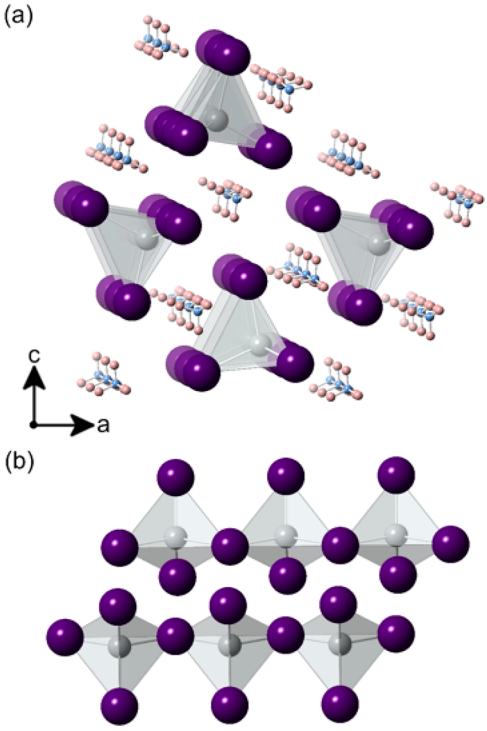

Figure 1. (a) Polyhedral model of the 1D structure of $(NH_4)_2AgX_3$ projected down the *b*-axis. (b) Isolated tetrahedral chains of $^1_\infty[AgX_3]^{2-}$ demonstrating the 1D connectivity of corner-sharing AgX_4 tetrahedra. Silver, halide, nitrogen, and hydrogen are colored in gray, purple, blue, and pink, respectively.

Large single crystals of $(NH_4)_2AgBr_3$ and $(NH_4)_2AgI_3$ measuring up to 1.5 cm long are effortlessly obtained through a hydrothermal process (Figure S1). However, the obtained crystals can be contaminated with small amounts of impurity crystals of binary AgX on the surface, which can be mechanically separated and washed off the $(NH_4)_2AgX_3$ crystals. To confirm the bulk purity of resultant samples, a portion of these crystals was thoroughly ground for room temperature PXRD measurements (Figure S2). Based on our PXRD results, mechanical separation with subsequent washing is effective in removing the surface AgX impurities. Since Ag^+ naturally photodegrades to Ag, the stability of the resultant compounds was monitored.[30] To evaluate their stability, the materials were stored under ambient air conditions for approximately 10 h/day between the PXRD scans. The environmental conditions were set at 20 °C and a relative humidity of 30%. Over 3 weeks, no significant signs of degradation were observed (Figure S3); however, a relatively small drop in peak intensities was recorded. The fact that the sample purity is preserved when kept in air for 2 weeks is a significant improvement over the stability demonstrated by the related copper(I) halides such as Rb_2CuCl_3.[13] Previous studies of copper halides have shown that, over time, copper often oxidizes into the divalent state.[13,14] Here, we observe potential practical benefits of replacing Cu(I) with Ag(I) in high-efficiency light-emitting group 11 elements; unlike Cu(I), Ag(I) is less likely to oxidize in air, which results in the enhanced air stability of Ag(I) halides.

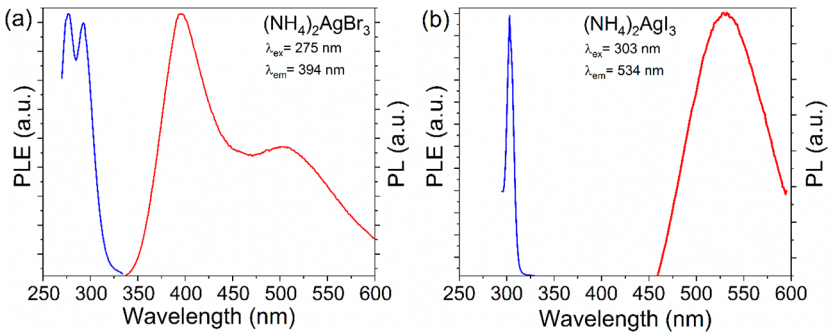

Figure 2. Room temperature photoluminescence excitation (PLE, blue lines) and photoluminescence emission (PL, red lines) spectra of single crystals of (a) $(NH_4)_2AgBr_3$ and (b) $(NH_4)_2AgI_3$.

https://doi.org/10.1021/acsmaterialsau.1c00009
ACS Mater. Au XXXX, XXX, XXX−XXX

To evaluate the thermal stability of $(NH_4)_2AgBr_3$ and $(NH_4)_2AgI_3$, simultaneous TGA and DSC measurements were performed (Figure S4). The results are consistent with other compounds in the A_2AgX_3 and A_2CuX_3 families; a single distinct thermal event is seen for $(NH_4)_2AgI_3$ at 272.44 °C. For $(NH_4)_2AgBr_3$, there is a similar event at 259.22 °C and a second event at 416.49 °C. The first thermal event is hypothesized to be a peritectic decomposition point, which is accompanied by the evaporation and loss of the ammonium salt. The weight loss of 42% and 55% at 272.44 and 259.22 °C approximately matches the 51% and 55% weight of the ammonium salt (NH_4Br and NH_4I, respectively) in $(NH_4)_2AgBr_3$ and $(NH_4)_2AgI_3$, respectively. For $(NH_4)_2AgBr_3$, the second event at 416.49 °C is hypothesized to be the melting transition of the residual ammonium bromide and silver bromide mixture. This conjecture is based on the approximation of the second point to the respective silver halide melting point.

To evaluate the optical properties of $(NH_4)_2AgX_3$, room-temperature photoluminescence excitation (PLE) and photoluminescence emission (PL) were measured for both compounds (Figure 2). Immediately noticeable is that the PL and PLE plots are different for $(NH_4)_2AgBr_3$ and $(NH_4)_2AgI_3$. While significant changes in the PL properties of all-inorganic lead halides such as $CsPbX_3$ occur upon halogen substitution, A_2CuX_3 are known as efficient and narrow blue emitters with a lack of tunability of their PL properties.[2,4,8,13,14,17,18] This unusually weak dependence of light emission properties of A_2CuX_3 on the halogen site substitutions has been explained by the fact that conduction band minimum (CBM) and valence band maximum (VBM) are dominated by Cu(I) orbitals in their electronic band structures.[13,14,20] The substitution of Cu(I) with Ag(I) is, therefore, expected to directly impact the bands around the optical gap, changing orbital contributions to the VBM and CBM, and consequently resulting in significant changes to the observed PL properties of $(NH_4)_2AgX_3$ in comparison to their Cu(I) analogues.

In the present case, $(NH_4)_2AgBr_3$ has a broad white emission, with a maximum at 394 nm and a shoulder peak at 524 nm, and the corresponding PLE plot shows two maxima at 275 and 290 nm. The two excitation transitions are also clearly seen in the diffuse reflectance plots measured on polycrystalline powder samples (Figure S5a). In comparison, $(NH_4)_2AgI_3$ has only a single lower-energy PL peak with a maximum at 534 nm with a corresponding PLE peak at 303 nm. Note that the diffuse reflectance spectra for $(NH_4)_2AgBr_3$ and $(NH_4)_2AgI_3$ feature small transitions at ∼2.5 and 2.8 eV, respectively, attributed to the presence of surface impurities of AgBr and AgI, respectively. As-prepared samples have more pronounced features in this region, however, with careful crystal selection, mechanical separation and repeated washing, these absorption bands are largely suppressed, albeit not eliminated completely.

The presence of two PL peaks for $(NH_4)_2AgBr_3$ is indicative of a multiple emission centers, specifically the presence of a higher energy self-trapped exciton (STE) and a lower energy defect-bound (DBE) emission, analogous to the PL properties reported for Rb_2AgBr_3.[21] Furthermore, unlike the PL plot for $(NH_4)_2AgBr_3$, there is no higher energy peak for $(NH_4)_2AgI_3$, indicating a single emission mechanism attributed solely to DBEs located on iodine vacancies within the tetrahedral chains. Therefore, the halogen-dependence of emission properties of silver halides is explained by the fact that the halogen vacancies (V_{Br}) have been shown to trap excitons leading to DBE emission in Rb_2AgBr_3. Similarly, starkly different photoemission properties have been reported for Cs_2AgCl_3 and Cs_2AgBr_3.[22]

For both $(NH_4)_2AgX_3$ compounds, the PLE plots are comparable to those of K_2CuCl_3 and K_2CuBr_3, which show maxima at 291 and 296 nm, respectively. The notable broadness of the PL peaks for the $(NH_4)_2AgX_3$ compounds results in a visible white or near-white light emission. Namely, $(NH_4)_2AgBr_3$ has a significantly broader emission with a full width at half-maximum (fwhm) value of 142 nm compared to the fwhm of 54 nm reported for A_2CuX_3.[13,14] $(NH_4)_2AgI_3$ has a slightly smaller fwhm of 114 nm due to the presence of a single PL peak; however, this fwhm value is still more than twice that of the blue-emitting copper(I) halides (Table 1).

Table 1. Comparison of the Photophysical Properties of Ternary A_2MX_3 (A = K, Rb, Cs; M = Cu, Ag; X = Cl, Br, I)[4,13,14,22]

compd	PL_{max} (nm)	PLE_{max} (nm)	Stokes shift (nm)	lifetime (μs)	fwhm (nm)	ref
$(NH_4)_2AgBr_3$	394	275	119	0.995	142	this work
$(NH_4)_2AgI_3$	534	303	231	1.25	114	this work
Cs_2AgCl_3	397	250	147	0.068		22
Cs_2AgBr_3	524	292	232	0.114		22
Cs_2AgI_3	595	310	285	0.135		22
K_2CuCl_3	392	291	101	12.97	54	13
K_2CuBr_3	388	296	92		54	13
Rb_2CuCl_3	400	300	100	12.21	52	14
Rb_2CuBr_3	385	300	85		∼54	4

The broadness of these peaks further supports the attribution of DBEs as the emission mechanism as opposed to narrower STE peaks observed in the analogous Cu(I) compounds.[4,13,14,18,31,32] The narrower emission peak for $(NH_4)_2AgI_3$ yields a greenish-white emission color with the Commission Internationale de l'Eclairage (CIE) color coordinates of (0.23, 0.53) compared to the white emission with the CIE coordinates of (0.25, 0.36) by $(NH_4)_2AgBr_3$. Based on these CIE coordinates, a correlated color temperature value of 9273 K is calculated for $(NH_4)_2AgBr_3$. CIE 1931 plots generated from PL emission spectra can be found in Figure S6. Finally, the Stokes shifts of $(NH_4)_2AgBr_3$ and $(NH_4)_2AgI_3$ are 119 and 231 nm, respectively, which are comparable to the Stokes shifts demonstrated by other analogous low-dimensional metal halides with excitonic light emission properties (Table 1).

In addition to stark differences to the PL properties of Cu(I) halides, we also note distinct variation of light emission properties in Ag(I) halides depending on the A site cation, e.g., $(NH_4)_2AgBr_3$, Rb_2AgBr_3, and Cs_2AgBr_3 have PL emission peaks at 394, 484, and 518 nm, respectively. Similarly, the PL spectra of $(NH_4)_2AgI_3$, Rb_2AgI_3, and Cs_2AgI_3 feature peaks at 534, 483, and 579 nm, respectively. Such sensitivity of light emission properties of low-dimensional ternary metal halides on the A cation site is unusual as A site cations typically have no direct contribution to the states in the vicinity of the optical band gap. Here, both for bromides and iodides, PLE peak positions are largely identical, but both PL peak positions and

https://doi.org/10.1021/acsmaterialsau.1c00009
ACS Mater. Au XXXX, XXX, XXX−XXX

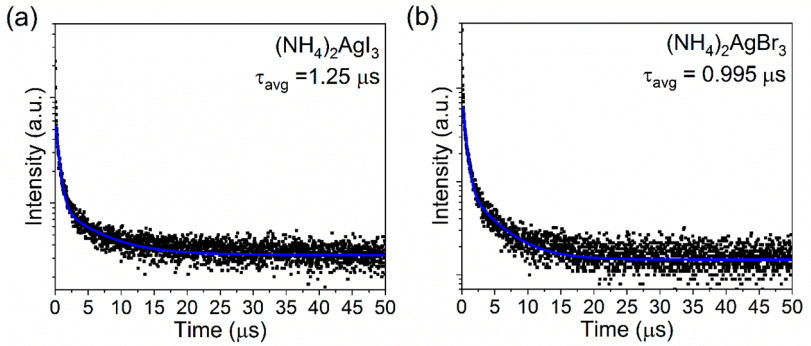

Figure 3. Time-resolved PL plots for (a) $(NH_4)_2AgBr_3$ and (b) $(NH_4)_2AgI_3$ measured using a 299 nm excitation source.

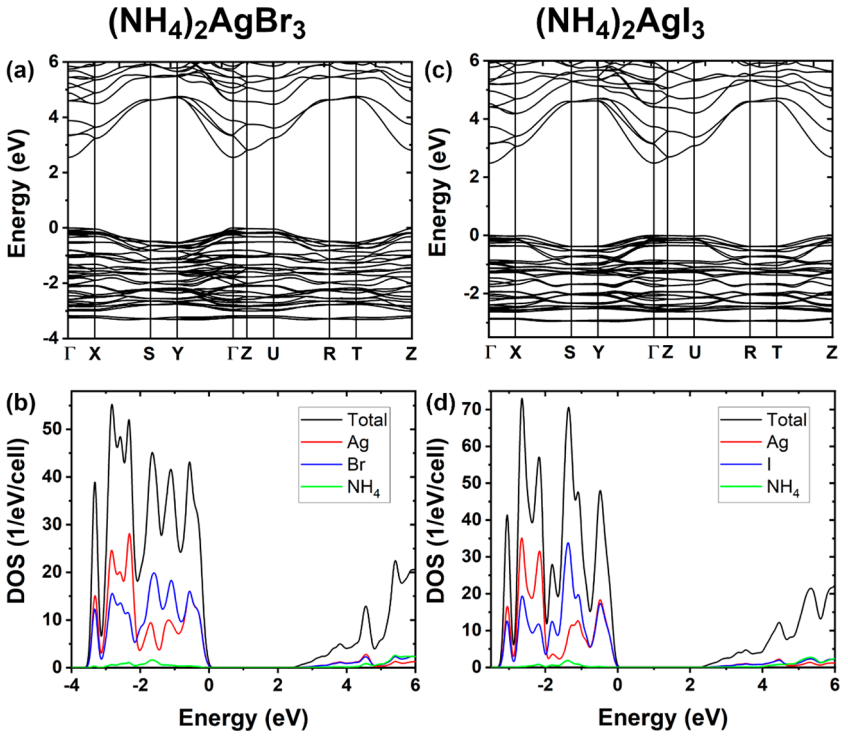

Figure 4. Electronic band structures and DOS of (a,b) $(NH_4)_2AgBr_3$ and (c,d) $(NH_4)_2AgI_3$.

shapes as evidenced by the varying fwhm values are strongly dependent on the nature of the A cation. We attribute the observed impact of the A cations such as NH_4^+ to their hydrogen bonding capabilities, which can impact the local coordination around the B metal cation, leading to starkly different PL emission properties. Similar observations are made by comparing the reported PL properties of hybrid organic–inorganic copper halides such as green-emitting $(MA)_4Cu_2Br_6$ and all-inorganic copper halides such as blue-emitting Rb_2CuBr_3.[33]

To further probe the photoluminescence emission mechanism of the $(NH_4)_2AgX_3$ compounds, additional photoluminescence spectroscopy measurements were performed. First, surface defects as the source of emission were ruled out. Single crystals were ground with PL taken before and after grinding (Figure S7), which showed only a decrease in emission intensities, ruling out surface defects as the significant source of PL emission in these compounds. Instead, we observe a nearly 2-fold reduction in PL intensity for powder samples, suggesting the presence of surface trap states that may quench PL. A comparison of crystal grain size before and after grinding is provided in Figure S8. Excitation wavelength-dependent emission was done to determine whether multiple emission mechanisms were at play. For $(NH_4)_2AgBr_3$, there is a loss of intensity in the lower energy excitation peak when the excitation energy is lowered (Figure S9), suggesting a multiexcitonic nature of emission; the emission primarily varies in the lower energy peak, and this is consistent with the assignment of this peak to DBEs. However, the PL emission profile does not change with excitation energy for $(NH_4)_2AgI_3$, suggesting an only DBE-based photoemission mechanism for this material (Figure S10). Next, time-resolved PL was done, in which a two-exponential fitting was used to determine the average lifetimes of PL emission for $(NH_4)_2AgX_3$, which yields similar average lifetimes of 0.995 and 1.25 μs for $(NH_4)_2AgBr_3$ and $(NH_4)_2AgI_3$, respectively, shown in Figure 3. While these values are approximately 1/10 of the lifetimes reported for the related A_2CuX_3 single crystals, they are significantly longer than fast emission lifetimes expected for a singlet emission from free exciton recombination.

https://doi.org/10.1021/acsmaterialsau.1c00009
ACS Mater. Au XXXX, XXX, XXX−XXX

Electronic band structures and DOS of $(NH_4)_2AgX_3$ (X = Br, I) obtained by PBE calculations are shown in Figure 4. Both compounds exhibit a direct band gap at the Γ point. The calculated PBE band gaps are 2.55 and 2.49 eV for $(NH_4)_2AgBr_3$ and $(NH_4)_2AgI_3$, respectively; they are corrected by the hybrid PBE0 calculation to 4.58 and 4.50 eV. The projected DOS in Figure 4 shows that the conduction band of $(NH_4)_2AgX_3$ is made up of Ag-5*s* orbitals, which hybridize with halogen-*p* orbitals, while the valence band is a mixing of Ag-4*d* and halogen-*p* states. The hybridization between Ag-4*d* and halogen-*p* in $(NH_4)_2AgX_3$ is significantly stronger than that between Cu-3*d* and halogen-*p* in Rb_2CuX_3 and K_2CuX_3.[13,14] This stronger contribution opens the door for further halide tunability of emission spectra for similar ternary silver halides. The band gaps follow the normal decreasing trend from $(NH_4)_2AgBr_3$ to $(NH_4)_2AgI_3$, consistent with the red shift of excitation energies observed in the experiment.

CONCLUSION

We report the hydrothermal synthesis and broadband white light emission properties of $(NH_4)_2AgX_3$ (X = Br, I), which are substitution analogues of the ultrabright blue-emitting A_2CuX_3 family. Unlike the A_2CuX_3 family, $(NH_4)_2AgX_3$ are shown to exhibit light emission properties that are sensitive to A and X site substitutions. The tunability of photoemission in $(NH_4)_2AgX_3$ through halogen substitution is explained by the greater contribution of the halogen-*p* states to the valence and conduction bands. In addition, $(NH_4)_2AgBr_3$ exhibits a dual emission mechanism attributed to self-trapped excitons and bromine vacancy V_{Br} bound excitons. The presence of multiple emission peaks for $(NH_4)_2AgBr_3$ results in broad PL emission spectra covering the entire visible spectrum yielding white emission with the CIE coordinates of (0.25, 0.36). Our combined experimental and theoretical work on $(NH_4)_2AgX_3$ suggests that substitution of Cu(I) with Ag(I) in A_2CuX_3 not only provides a route for PL tunability but also significantly improves the materials' stability. In conclusion, ternary silver halides are attractive alternatives to toxic lead halide perovskites and unstable copper(I) halides.

ASSOCIATED CONTENT

Supporting Information

The Supporting Information is available free of charge at https://pubs.acs.org/doi/10.1021/acsmaterialsau.1c00009.

Sample photos, single crystal and powder X-ray diffraction results, DSC/TGA, diffuse reflectance, ground samples versus single crystals PL, ESEM images, and excitation wavelength-dependent PL (PDF)

AUTHOR INFORMATION

Corresponding Author

Bayram Saparov − *Department of Chemistry and Biochemistry, University of Oklahoma, Norman, Oklahoma 73019, United States;* orcid.org/0000-0003-0190-9585; Email: saparov@ou.edu

Authors

Tielyr D. Creason − *Department of Chemistry and Biochemistry, University of Oklahoma, Norman, Oklahoma 73019, United States*

Hadiah Fattal − *Department of Chemistry and Biochemistry, University of Oklahoma, Norman, Oklahoma 73019, United States*

Isaiah W. Gilley − *Department of Chemistry and Biochemistry, University of Oklahoma, Norman, Oklahoma 73019, United States*

Timothy M. McWhorter − *Department of Chemistry and Biochemistry, University of Oklahoma, Norman, Oklahoma 73019, United States*

Mao-Hua Du − *Materials Science & Technology Division, Oak Ridge National Laboratory, Oak Ridge, Tennessee 37830, United States;* orcid.org/0000-0001-8796-167X

Complete contact information is available at: https://pubs.acs.org/10.1021/acsmaterialsau.1c00009

Author Contributions

[§]T.D.C. and H.F. contributed equally. The manuscript was written through the contributions of all authors. All authors have approved the final version of the manuscript. T.D.C., H.F., T.M.M., and I.W.G. prepared the samples. T.D.C. and H.F. performed PXRD, TGA/DSC measurements, performed and analyzed the optical measurements, M.-H.D. carried out the theoretical calculations, and B.S. conceived and supervised the work.

Notes

The authors declare no competing financial interest.

This paper has been coauthored by UT-Battelle, LLC under Contract No. DE-AC05-00OR22725 with the U.S. Department of Energy. The United States Government retains and the publisher, by accepting the article for publication, acknowledges that the United States Government retains a nonexclusive, paid-up, irrevocable, worldwide license to publish or reproduce the published form of this manuscript, or allow others to do so, for United States Government purposes. The Department of Energy will provide public access to these results of federally sponsored research in accordance with the DOE Public Access Plan (http://energy.gov/downloads/doe-public-access-plan).

ACKNOWLEDGMENTS

This material is based upon work supported by the National Aeronautics and Space Administration under Agreement No. 80NSSC19M0140 issued through NASA Oklahoma EPSCoR. M.-H.D. was supported by the U.S. Department of Energy, Office of Science, Basic Energy Sciences, Materials Sciences, and Engineering Division. We thank Dr. Douglas R. Powell for his help with the single-crystal X-ray diffraction measurements (supported by NSF grant CHE-1726630).

REFERENCES

(1) Mo, X.; Li, T.; Huang, F.; Li, Z.; Zhou, Y.; Lin, T.; Ouyang, Y.; Tao, X.; Pan, C. Highly-efficient all-inorganic lead-free 1D CsCu2I3 single crystal for white-light emitting diodes and UV photodetection. *Nano Energy* **2021**, *81*, 105570.

(2) Dou, L.; Lai, M.; Kley, C. S.; Yang, Y.; Bischak, C. G.; Zhang, D.; Eaton, S. W.; Ginsberg, N. S.; Yang, P. Spatially resolved multicolor CsPbX3 nanowire heterojunctions via anion exchange. *Proc. Natl. Acad. Sci. U. S. A.* **2017**, *114*, 7216.

(3) Lin, Y.-C.; Karlsson, M.; Bettinelli, M. Inorganic Phosphor Materials for Lighting. *Top. Curr. Chem.* **2016**, *374* (2), 21.

(4) Yang, B.; Yin, L.; Niu, G.; Yuan, J.-H.; Xue, K.-H.; Tan, Z.; Miao, X.-S.; Niu, M.; Du, X.; Song, H.; Lifshitz, E.; Tang, J. Lead-Free

Halide Rb2CuBr3 as Sensitive X-Ray Scintillator. *Adv. Mater.* **2019**, *31* (44), 1904711.
(5) Nikl, M.; Yoshikawa, A. Recent R&D Trends in Inorganic Single-Crystal Scintillator Materials for Radiation Detection. *Adv. Opt. Mater.* **2015**, *3* (4), 463−481.
(6) Zhang, F.; Zhong, H.; Chen, C.; Wu, X.-g.; Hu, X.; Huang, H.; Han, J.; Zou, B.; Dong, Y. Brightly Luminescent and Color-Tunable Colloidal CH3NH3PbX3 (X = Br, I, Cl) Quantum Dots: Potential Alternatives for Display Technology. *ACS Nano* **2015**, *9* (4), 4533−4542.
(7) Dai, X.; Deng, Y.; Peng, X.; Jin, Y. Quantum-Dot Light-Emitting Diodes for Large-Area Displays: Towards the Dawn of Commercialization. *Adv. Mater.* **2017**, *29* (14), 1607022.
(8) Wei, Y.; Cheng, Z.; Lin, J. An overview on enhancing the stability of lead halide perovskite quantum dots and their applications in phosphor-converted LEDs. *Chem. Soc. Rev.* **2019**, *48* (1), 310−350.
(9) Yang, Z.; Gao, M.; Wu, W.; Yang, X.; Sun, X. W.; Zhang, J.; Wang, H.-C.; Liu, R.-S.; Han, C.-Y.; Yang, H.; Li, W. Recent advances in quantum dot-based light-emitting devices: Challenges and possible solutions. *Mater. Today* **2019**, *24*, 69−93.
(10) Ono, L. K.; Qi, Y.; Liu, S. Progress toward Stable Lead Halide Perovskite Solar Cells. *Joule* **2018**, *2* (10), 1961−1990.
(11) Wu, M.; Haji Ladi, N.; Yi, Z.; Li, H.; Shen, Y.; Wang, M. Stability Issue of Perovskite Solar Cells under Real-World Operating Conditions. *Energy Technol. (Weinheim, Ger.)* **2020**, *8* (4), 1900744.
(12) Huang, H.; Susha, A. S.; Kershaw, S. V.; Hung, T. F.; Rogach, A. L. Control of Emission Color of High Quantum Yield CH3NH3PbBr3 Perovskite Quantum Dots by Precipitation Temperature. *Advanced Science* **2015**, *2* (9), 1500194.
(13) Creason, T. D.; Yangui, A.; Roccanova, R.; Strom, A.; Du, M.-H.; Saparov, B. Rb2CuX3 (X = Cl, Br): 1D All-Inorganic Copper Halides with Ultrabright Blue Emission and Up-Conversion Photoluminescence. *Adv. Opt. Mater.* **2020**, *8* (2), 1901338.
(14) Creason, T. D.; McWhorter, T. M.; Bell, Z.; Du, M.-H.; Saparov, B. K2CuX3 (X = Cl, Br): All-Inorganic Lead-Free Blue Emitters with Near-Unity Photoluminescence Quantum Yield. *Chem. Mater.* **2020**, *32* (14), 6197−6205.
(15) Roccanova, R.; Yangui, A.; Nhalil, H.; Shi, H.; Du, M.-H.; Saparov, B. Near-Unity Photoluminescence Quantum Yield in Blue-Emitting $Cs_3Cu_2Br_{5-x}I_x$ ($0 \le x \le 5$). *ACS Appl. Electron. Mater.* **2019**, *1* (3), 269−274.
(16) Jun, T.; Sim, K.; Iimura, S.; Sasase, M.; Kamioka, H.; Kim, J.; Hosono, H. Lead-Free Highly Efficient Blue-Emitting Cs3Cu2I5 with 0D Electronic Structure. *Adv. Mater.* **2018**, *30* (43), 1804547.
(17) Zhao, X.; Niu, G.; Zhu, J.; Yang, B.; Yuan, J.-H.; Li, S.; Gao, W.; Hu, Q.; Yin, L.; Xue, K.-H.; Lifshitz, E.; Miao, X.; Tang, J. All-Inorganic Copper Halide as Stable and Self-Absorption Free X-Ray Scintillator. *J. Phys. Chem. Lett.* **2020**, *11* (5), 1873−1880.
(18) Gao, W.; Yin, L.; Yuan, J.-H.; Xue, K.-H.; Niu, G.; Yang, B.; Hu, Q.; Liu, X.; Tang, J. Lead-free violet-emitting K2CuCl3 single crystal with high photoluminescence quantum yield. *Org. Electron.* **2020**, *86*, 105903.
(19) Li, S.; Luo, J.; Liu, J.; Tang, J. Self-Trapped Excitons in All-Inorganic Halide Perovskites: Fundamentals, Status, and Potential Applications. *J. Phys. Chem. Lett.* **2019**, *10*, 1999−2007.
(20) Du, M.-H. Emission Trend of Multiple Self-Trapped Excitons in Luminescent 1D Copper Halides. *ACS Energy Lett.* **2020**, *5* (2), 464−469.
(21) Zhang, M.; Wang, X.; Yang, B.; Zhu, J.; Niu, G.; Wu, H.; Yin, L.; Du, X.; Niu, M.; Ge, Y.; Xie, Q.; Yan, Y.; Tang, J. Metal Halide Scintillators with Fast and Self-Absorption-Free Defect-Bound Excitonic Radioluminescence for Dynamic X-Ray Imaging. *Adv. Funct. Mater.* **2021**, *31* (9), 2007921.
(22) Zhang, Z.; Zhao, R.; Teng, S.; Huang, K.; Zhang, L.; Wang, D.; Yang, W.; Xie, R.; Pradhan, N. Color Tunable Self-Trapped Emissions from Lead-Free All Inorganic IA-IB Bimetallic Halides Cs-Ag-X (X = Cl, Br, I). *Small* **2020**, *16* (44), 2004272.
(23) Sun, C.; Guo, Y.-H.; Yuan, Y.; Chu, W.-X.; He, W.-L.; Che, H.-X.; Jing, Z.-H.; Yue, C.-Y.; Lei, X.-W. Broadband White-Light Emission in One-Dimensional Organic−Inorganic Hybrid Silver Halide. *Inorg. Chem.* **2020**, *59* (7), 4311−4319.
(24) Hull, S.; Berastegui, P. Crystal structures and ionic conductivities of ternary derivatives of the silver and copper monohalides—II: ordered phases within the (AgX)x−(MX)1−x and (CuX)x−(MX)1−x (M = K, Rb and Cs; X = Cl, Br and I) systems. *J. Solid State Chem.* **2004**, *177* (9), 3156−3173.
(25) Kresse, G.; Furthmüller, J. Efficiency of ab-initio total energy calculations for metals and semiconductors using a plane-wave basis set. *Comput. Mater. Sci.* **1996**, *6* (1), 15−50.
(26) Kresse, G.; Joubert, D. From ultrasoft pseudopotentials to the projector augmented-wave method. *Phys. Rev. B: Condens. Matter Mater. Phys.* **1999**, *59* (3), 1758.
(27) Perdew, J. P.; Burke, K.; Ernzerhof, M. Generalized gradient approximation made simple. *Phys. Rev. Lett.* **1996**, *77* (18), 3865.
(28) Perdew, J. P.; Ernzerhof, M.; Burke, K. Rationale for mixing exact exchange with density functional approximations. *J. Chem. Phys.* **1996**, *105* (22), 9982−9985.
(29) Thackeray, M. M.; Coetzer, J. Dipotassium silver triiodide. *Acta Crystallogr., Sect. B: Struct. Crystallogr. Cryst. Chem.* **1975**, *31* (9), 2339−2340.
(30) Trivelli, A. P. H.; Sheppard, S. E. On the Visible Decomposition of Silver Halide Grains by Light. *J. Phys. Chem.* **1925**, *29* (12), 1568−1582.
(31) Zhao, X.; Niu, G.; Zhu, J.; Yang, B.; Yuan, J.-H.; Li, S.; Gao, W.; Hu, Q.; Yin, L.; Xue, K.-H.; Lifshitz, E.; Miao, X.; Tang, J. All-Inorganic Copper Halide as a Stable and Self-Absorption-Free X-ray Scintillator. *J. Phys. Chem. Lett.* **2020**, *11* (5), 1873−1880.
(32) Gao, W.; Niu, G.; Yin, L.; Yang, B.; Yuan, J.-H.; Zhang, D.; Xue, K.-H.; Miao, X.; Hu, Q.; Du, X.; Tang, J. One-Dimensional All-Inorganic K2CuBr3 with Violet Emission as Efficient X-ray Scintillators. *ACS Applied Electronic Materials* **2020**, *2* (7), 2242−2249.
(33) Peng, H.; Yao, S.; Guo, Y.; Zhi, R.; Wang, X.; Ge, F.; Tian, Y.; Wang, J.; Zou, B. Highly Efficient Self-Trapped Exciton Emission of a (MA)4Cu2Br6 Single Crystal. *J. Phys. Chem. Lett.* **2020**, *11* (12), 4703−4710.

https://doi.org/10.1021/acsmaterialsau.1c00009
ACS Mater. Au XXXX, XXX, XXX−XXX